Journal of Medicinal Chemistry

Subscriber access provided by American Chemical Society

Article

Is Antagonism of *E*/*Z*-Guggulsterone at the Farnesoid X Receptor Mediated by a Noncanonical Binding Site? A Molecular Modeling Study

Udo Meyer, Gabriele Costantino, Antonio Macchiarulo, and Roberto Pellicciari

J. Med. Chem., **2005**, 48 (22), 6948-6955• DOI: 10.1021/jm0505056 • Publication Date (Web): 08 October 2005

Downloaded from http://pubs.acs.org on March 29, 2009

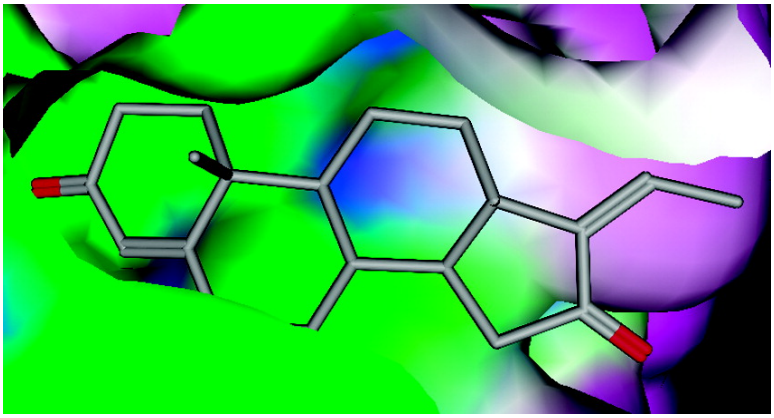

More About This Article

Additional resources and features associated with this article are available within the HTML version:

- Supporting Information
- Links to the 2 articles that cite this article, as of the time of this article download
- Access to high resolution figures
- Links to articles and content related to this article
- Copyright permission to reproduce figures and/or text from this article

View the Full Text HTML

ACS Publications
High quality. High impact.

Journal of Medicinal Chemistry is published by the American Chemical Society. 1155 Sixteenth Street N.W., Washington, DC 20036

Is Antagonism of *E*/*Z*-Guggulsterone at the Farnesoid X Receptor Mediated by a Noncanonical Binding Site? A Molecular Modeling Study

Udo Meyer, Gabriele Costantino, Antonio Macchiarulo, and Roberto Pellicciari*

Dipartimento di Chimica e Tecnologia del Farmaco, Università di Perugia, Via del Liceo 1, I-06123 Perugia, Italy

Received May 31, 2005

Guggulsterone **1**, the active principle of guggulipid, has been used in ethnic medicine for thousands of years for its antinflammatory and antilipidemic activities. The activities of **1** are apparently mediated by its interaction with an array of nuclear receptors, including endocrine steroid receptors and metabolic lipid receptors. Although relatively weak, the activity at the metabolic farnesoid X receptor (FXR) is particularly intriguing, as **1** is, so far, the only antagonist known for this receptor, with a peculiar ability of gene selective modulation. We report here a systematic study aimed at identifying the potential binding pocket of **1** at FXR. Although **1** could be docked into the canonical binding site, we identified a novel, so far undescribed binding pocket, localized near the loop region between helix 1 and helix 2. This novel binding pocket may explain some of the peculiar characteristics of **1** when acting at FXR.

Introduction

Guggulsterones [*Z*- and *E*-4,17(20)-pregnadiene-3,16-dione, **1a** and **1b**, respectively (Chart 1)], constitute the active principle of guggulipid, the ethyl acetate extract of the gum resin of *Commiphora mukul*, known in ayurvedic medicine since 600 BC.[1,2] A variety of activities have been associated with the use of guggulipid, including antiseptic, antirheumatic, and antinflammatory properties. Furthermore, weight loss, uterine-stimulant, expectorant, astringent, and thermogenesis effects have been described.[3] Most of the interest in the use of guggulipid, however, has been focused on its effect on lipid metabolism, as guggulipid has been found to reduce triglyceride levels as well as the total and the LDL cholesterol, although these data have been recently questioned.[4,5]

Several studies have indicated that many of the observed properties of guggulipid can be ascribed to the interaction of its active principle, **1**, with an array of nuclear receptors (NR).[6−10] Thus, both *Z*- and *E*-guggulsterone (**1a** and **1b**) have been shown to interact with the members of the subfamily of endocrine NRs, such as the α-isoform of the estrogen receptor (ER, NR3A1), the progesterone receptor (PR, NR3C3), the androgen receptor (AR, NR3C4), the glucorticoid receptor (GR, NR3C1), and the mineralcorticoid receptor (MR, NR3C2) (Table 1).[6] Furthermore, **1** has also been found to interact with members of the subfamily of the formerly orphan metabolic NRs, such as the pregnane X receptor (PXR, NR1I2) and the bile acid receptor, the farnesoid X receptor (FXR, NR1H4).[7−10]

Among the activities of **1** at NRs, the latter is certainly an intriguing one. Indeed, FXR is a transcriptional sensor activated by bile acids (Chart 2), chenodeoxycholic acid (CDCA, **2**) being the most potent endogenous activator.[11] FXR controls expression of genes crucial for bile acid synthesis as well as for cholesterol homeostasis and is potently activated by the synthetic steroid agonist 6ECDCA (INT-747, **6**) and by the nonsteroid agonists GW4064 (**7**) and fexeramine (**8**).[12−19]

Chart 1

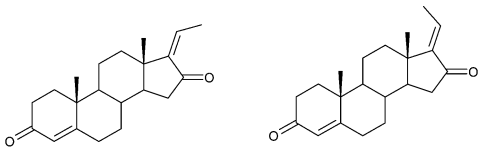

It has been shown, in particular, that FXR controls bile acid synthesis by inhibiting the expression of cholesterol 7α-hydroxylase and sterol 12α-hydroxylase genes.[20,21] It furthermore controls the bile acid transport by regulating the expression of the critical hepatic bile Na^+/taurocholate cotransporting polypeptide, the bile salt export pump (BSEP), and the phospholipid transporters MDR3 and MRP2.[22−26] Finally FXR controls the expression of the intestinal bile acid binding protein, the phospholipid transfer protein, the apolipoproteins A-I, C-II, and C-III and was also reported to activate the expression of human kininogen gene, the products of which have crucial roles in vasodilatation and anticoagulation.[27−31] It was recently proposed that a FXR-SHP regulatory cascade promotes resolution of liver fibrosis, giving rise to the expectation that FXR ligands might represent a novel therapeutic option to treat liver fibrosis.[32]

The interaction of **1** with FXR is rather peculiar. In particular, **1** failed to activate FXR in a transactivation assay, while strongly inhibited the activation by **2** in concentrations above 10 μM.[8] In cell-free assay, **1** was unable to recruit a synthetic peptide corresponding to the GRIP-1 region of SRC-1 coactivator protein and reverted, in a dose-dependent manner, the recruitment of the peptide by **2** at approximately 80 μM.[27] Thus, **1** displayed an apparent profile of a FXR antagonist, the only one so far reported together with the semisynthetic 3β-hydroxy-5,16-pregnadien-20-one (80−574, **9**) and

Corresponding author. E-mail: rp@unipg.it, Phone: +39 075 585 5128, Fax: +39 075 585 5165.

10.1021/jm0505056 CCC: $30.25 © 2005 American Chemical Society
Published on Web 10/08/2005

Table 1. K_i Values and Activity of **1** in Diverse NRs[a]

NR	*Z*-guggulsterone (**1a**)		*E*-guggulsterone (**1b**)		activity
	K_i (nM)	EC_{50} or IC_{50} (nM)	K_i (nM)	EC_{50} or IC_{50} (nM)	
FXR (NR1H4)	>5000	50−100000	> 5000	50−100000	antagonist[b]
PXR (NR1I2)		2.4 (nsp)		2.4 (nsp)	agonist[c]
ERα (NR3A1)	>5000	>5000	>5000	>5000	agonist[b]
GR (NR3C1)	252 ± 2	6060 ± 310	224 ± 26	1740 ± 150	antagonist[b]
MR (NR3C2)	37 ± 2	1880 ± 390	39 ± 4	1000 ± 310	antagonist[b]
PR (NR3C3)	224 ± 6	740 ± 220	201 ± 18	1200	antagonist[b]
AR (NR3C4)	315 ± 13	660 ± 240	240 ± 21	220 ± 70	agonist[b]

[a] nsp: Nonspecified **1a** and **1b**. [b] K_i values reported by Burris, T. P.; Montrose, C. (2005).[7] [c] K_i values reported by Owsley, E.; Chiang, J. Y. (2003).[11]

Chart 2

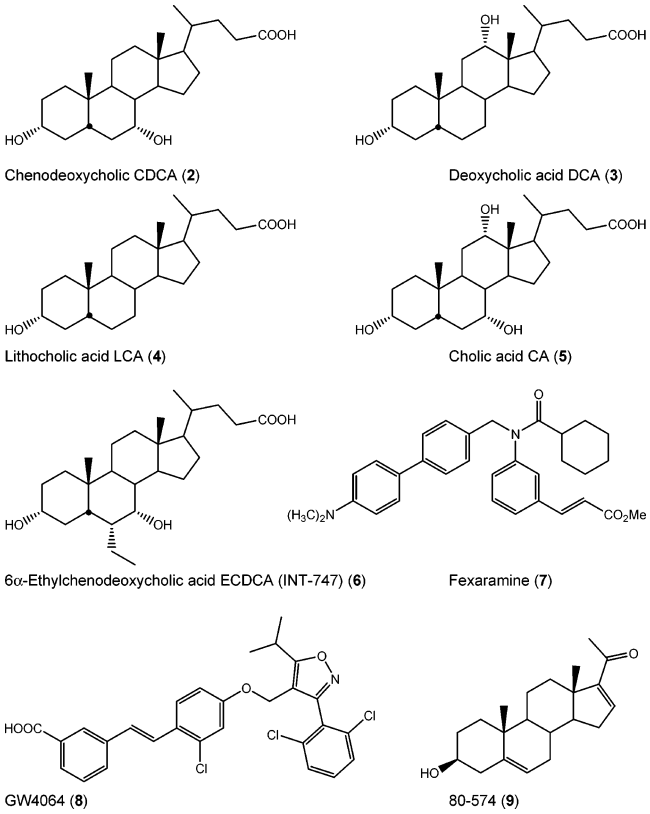

some polyunsaturated fatty acids.[9,33] It should be observed, however, that despite being characterized as a pure FXR antagonist in the coactivator association assay and shown to decrease the expression of bile acid activated genes, **1** was recently shown to enhance the FXR-agonist-induced expression of the bile salt export pump (BSEP), one of the target genes for FXR. Thus, **1** can be classified as a selective FXR modulator.

It is generally accepted that the coactivator association assay is a reliable predictor of the molecular interaction between a NR, its ligand, and the coactivator peptide. In this assay, **1** behaved as a pure antagonist. The molecular basis for the FXR antagonism elicited by **1** is however not easily understandable. Indeed, the classical concept for NR antagonism demands compounds larger than the endogenous activators, as they are supposed to induce conformational changes in the crucial H12 helix, thus shifting it from its active disposition to the inactive one.[34−36] Simple visual inspection indicates **1** as smaller than the endogenous agonist **2** or the potent synthetic agonist **6**. Thus, understanding the molecular basis for the antagonism of **1** at FXR requires more sophisticated explanation. In particular, we thought that the understanding of the binding mode of **1** may open the way to the rational design of undeveloped, selective FXR modulators. Thus, as a continuation of our work in the field of FXR modulators,[37−39] we present herein a study aimed at the clarification of the possible binding mode of **1** at FXR and the elucidation of its antagonist profile.

Table 2. Docking Energies (kcal/mol) and Abundancy of Docking Positions (% in parentheses) of the Docking Positions of **1a** and **1b** in the Two-Chain A Monomers of FXR

ligand	chain A: no coactivator		chain A: one coactivator	
	binding energy	position	binding energy	position
	Z-Guggulsterone (**1a**)			
Cluster 1	−10.9 (12)	S2	−11.0(10)	S2
Cluster 2	−10.5 (05)	S2	−10.5 (05)	S2
Cluster 3	−10.5 (14)	S1	−10.4 (14)	S1
Cluster 4	−10.4 (16)	S1	−10.4 (13)	S1
Cluster 5	−10.3 (05)	S1	−10.4 (06)	S1
	E-Guggulsterone (**1b**)			
Cluster 1	−12.1 (07)	S2	−12.2 (08)	S2
Cluster 2	−10.5 (10)	S1	−10.5 (12)	S1
Cluster 3	−10.5 (03)	S1	−10.3 (12)	S1
Cluster 4	−10.4 (29)	S1	−10.5 (05)	S1
Cluster 5	−10.3 (02)	S1	−09.7 (01)	S1

[a] Docking Position of **1a** in FXR and Docking Positions of **1b** in FXR According to Energy-Clustering. S1: Position Inside the Canonical Binding Site. S2: Position outside the Canonical Binding Site.

Experimental Strategy

Identification of the possible binding modes of **1** to FXR has been achieved by carrying out docking experiments on the crystal structure of rat FXR (rFXR), complexed with the bile acid agonist **6** (pdb: 1OSV), reported by Mi et al. in 2002.[40] This structure contains two monomers of the NR protein: the first one (chain A) is cocrystallized with a short peptide containing the conserved LxxLL motif of GRIP-1 coactivator. The peptide is localized in the canonical coactivator cleft. The second monomer (chain B) contains another cocrystallized peptide in addition to the canonical one, disposed in a newly described cleft along helices 1 and 2. To consider the potential mutual influence of the coactivator peptides on guggulsterone docking, we carried out a systematic analysis by studying both **1a** and **1b** in the following four receptor structures prepared from the crystal structure of 1OSV: (i) chain A without coactivator, (ii) chain A with one coactivator (Table 2), (iii) chain B without coactivators. and (iv) chain B with two coactivators (Table 3).

Protein Setup. Chains A and B of the crystal structure of LBD of FXR (pdb: 1OSV) were selected for

Table 3. Docking Energies (kcal/mol) and Abundancy of Docking Positions (% in parentheses) of the Docking Positions of **1a** and **1b** in the Two-Chain B Monomers of FXR[a]

	chain B: no coactivator		chain B: two coactivators	
ligand	docking energy	position	docking energy	position
	Z-Guggulsterone (**1a**)			
Cluster 1	−11.5 (10)	S1	−11.4 (06)	S1
Cluster 2	−11.3 (15)	S1	−11.3 (12)	S1
Cluster 3	−10.9 (01)	S1	−10.9 (01)	S1
Cluster 4	−10.6 (04)	S1	−10.6 (09)	S1
	E-Guggulsterone (**1b**)			
Cluster 1	−11.5 (11)	S1	−11.4 (11)	S1
Cluster 2	−11.0 (11)	S1	−11.0 (14)	S1
Cluster 3	−10.9(02)	S1	−10.9 (02)	S1
Cluster 4	−10.8 (01)	S1	−10.8 (01)	S1

[a] Docking position of **1a** in FXR and docking positions of **1b** in FXR according to energy-clustering. S1: Position inside the canonical binding site.

docking studies. The ligand and all the crystallized water molecules were deleted. Polar hydrogen atoms and Kollman charges were added using the Autodock-Tool program. Finally, solvation parameters were also added using the addsol utility included in AutoDock.

Ligand Preparation. The 3D structure of **6** extracted from 1OSV was used as a starting point for the preparation of the ligand, using the MOE program. Hydrogens were added and a geometry optimization was carried out with the CHARMM force field implemented in the MOE program, considering the ionized form of **6**. Appropriate modifications were performed to build up **1a** and **1b**, followed by the corresponding minimization. The so-optimized ligands were saved in a pdb format and transferred into the Autodock-Tools program. Gasteiger-Marsilii charges were added since this is the type of atomic charges used in the calibrating of the Autodock empirical force-field function. Finally, nonpolar hydrogens were merged in order to prepare the appropriate file for each docking study.

Docking Studies. Docking studies have been carried out with the Autodock 3.0.4 program, using the new empirical free energy function and the Lamarckian genetic algorithm. A standard protocol was used with 100 randomly placed starting relative positions of the ligands, a maximum of 1.5×10^6 energy evaluations and of 27000 generations, a mutation rate of 0.02, a crossover rate of 0.80, and an elitism value of 1. During the search, a 0.2 Å translation step was used while quaternion and torsion steps were fixed to a value of 5.0°. Proportional selection was used, calculating the average of the worst energy over a window of 10 generations. The so-called pseudo-Solis and Wets algorithm was used for the local search, with a maximum of 300 iterations. The probability of performing a local search of an individual was 0.06, and the maximum number of consecutive successes or failures before doubling or halving the local search step size was 4. The docking results were clustered using a rmsd. of 2.0 Å.

The grid maps representing the protein in the docking process were calculated using AutoGrid. The grids were chosen to be sufficiently large to include the binding site and a portion of the surrounding surface, to allow a completely free movement of the ligand inside the protein. A spacing of 0.375 Å and a dimension of 110 × 110 × 110 points, centered in the center of the crystal structure were chosen.

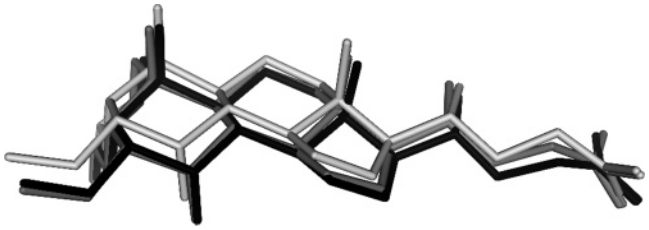

Figure 1. Docking positions of **6** of the lowest docking energy in FXR in comparison to the crystallized ligand (light gray: docking position of the lowest energy cluster of **6** in chain A without and (grey) with coactivator; dark gray: **6** in crystal structure of FXR).

Results

1. Visual Inspection. Before docking studies were performed, the differences between chain A and chain B in the crystal structure of the LBD of FXR were analyzed. Visual inspection of the superimposition of chain A on chain B revealed some differences. The rmsd between the two chains is 1.32 Å (calculated over the Cα·s). A significant difference can be appreciated in the side-chain's orientation of the loop region between helix 1 and helix 2 (loop H1−H2, residues K259−P263), where the rmsd (calculated over all the heavy atoms) is 2.48 Å. It should be mentioned that the difference between chain A and chain B of rFXR is low when compared to other known FXR structures. For instance the rmsd between the crystal structure of human and rat FXR is 2.684 Å, calculated over the Cα·s.

2. Characterization of the Ligands. 1a and **1b** are characterized by an *all trans* and quasi planar ABCD ring system, thus showing a planar, bipolar structure. The distance of the diametrically orientated enone carbonyl oxygens is 11.0 Å. **1** is therefore substantially shorter than the amphiphilic bile acids, which consist of a convex hydrophobic and a concave hydrophilic face. As a consequence, **1** has a smaller volume of 322 Å^3 compared to 439 Å^3 of **6**.

3. Control Docking Studies of 6. As a first step, we carried out docking experiments on **6** in order to verify whether the chosen docking's algorithm and settings are appropriate for reproducing the experimental disposition. Thus, when the agonist **6** was docked in chain A, four clusters were identified, while only one was found when docked in chain B. All the solutions found for either chain A or chain B are inside the canonical binding pocket (termed 'S1' hereinafter). The lowest energy docking positions for **6** in both chain A (E_{dock} = −14.5 kcal/mol, E_{bind} = −13.0 kcal/mol) and chain B (E_{dock} = −16.3 kcal/mol, E_{bind} = −15.0 kcal/mol) were identical to the position of the cocrystallized ligand in the crystal structures of chain A and chain B, respectively (Figure 1). The higher number of docking poses which is found in chain A with respect to chain B cannot be explained by the wider volume of the S1 binding pocket of chain A with respect to chain B (1072 and 1075 Å^3), but as a consequence of the slightly different orientation of the loop H1−H2. In particular, in chain B, this loop is pushed toward S1, and methionine 262 contacts the 24-carboxylate moiety of **6**. As a result of this contact, the docking energy of **6** is about

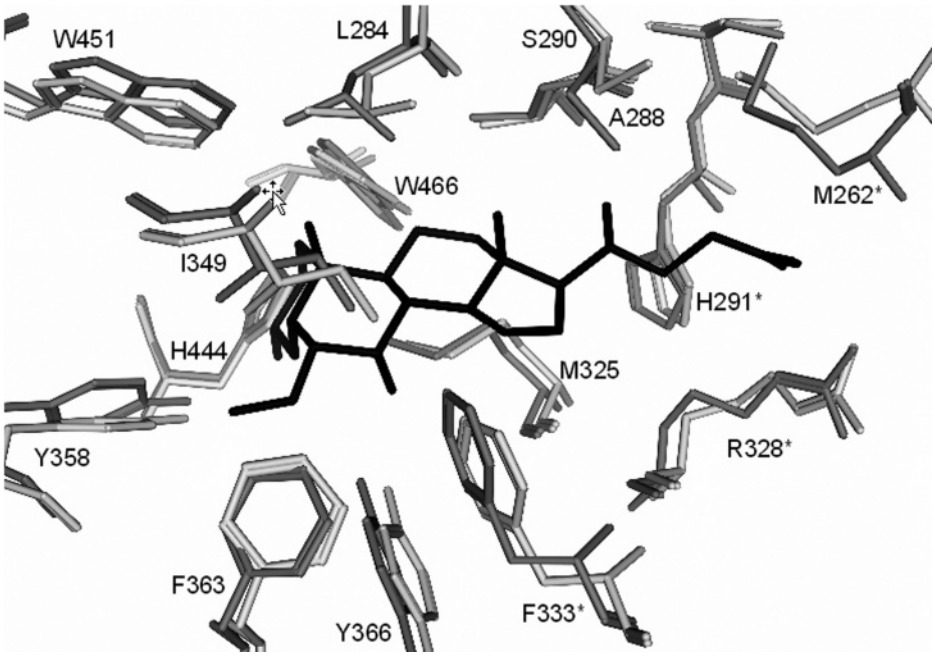

Figure 2. **6** (crystal data) in the canonical binding site S1 of chain A (light gray) and B (dark gray). The side chains of the residues forming the canonical binding site S1 in general show little difference between chain A and chain B, except for the residues M262 of the loop H1−H2 and R328 of helix 5. Residues with asterics (*) form a potential entrance channel near loop H1−H2.

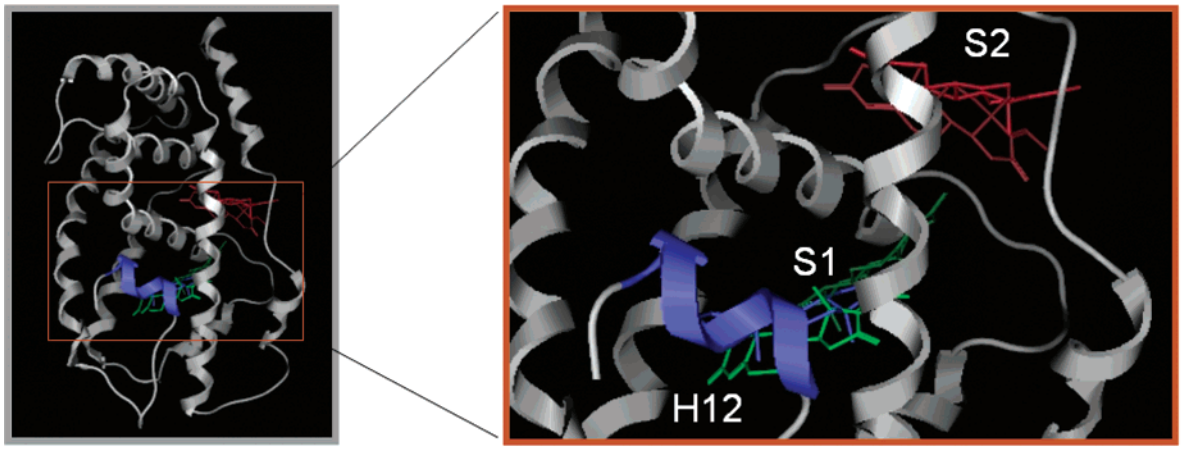

Figure 3. Docking positions of **1a** in FXR, chain A, experiment without coactivator protein. Left side: General view of the FXR chain A with docking positions of **1a**. Right side: Detailed view of the first and second cluster of **1a** in the canonical binding site S1 and of the third to fifth cluster inside the noncanonical binding site S2 (color code: light red: first cluster, dark red: second cluster, light green: third cluster, dark green: forth cluster, light blue: fifth cluster).

1.8 kcal/mol lower in value in chain B with respect to chain A (Figure 2).

4. Docking of 1a and 1b. When **1a** was docked into the four receptor systems, the most striking result was that in chain A, but not in chain B, two of the five obtained clusters were located outside the volume of the canonical binding site S1. Furthermore, these two 'noncanonical' poses are characterized by the lowest binding energy (Table 2). A qualitatively similar result was obtained with **1b**, for which the lowest energy disposition is located, in chain A, outside the canonical binding pocket S1 (Table 2). This alternative binding pocket found in chain A is herein termed 'noncanonical' binding pocket S2 (Figure 3).

Interestingly, for both **1a** and **1b**, docking experiments on chain B yielded four different dispositions, all of them located inside the canonical S1 binding pocket (Table 3). Inspection of Table 2 and Table 3 revealed that, in all the cases, the absolute binding energies predicted for docking poses inside the canonical binding pocket S1 are significantly lower than the corresponding binding energy calculated for the agonist **6**. Thus, the best predicted binding energies for **1a** in the S1 pocket of chain A and chain B are −10.5 kcal/mol and −11.5 kcal/mol, respectively, compared to −13.0 kcal/mol and −15.0 kcal/mol, respectively, calculated for **6**. Similarly, the best predicted binding energies for **1b** in the S1 pocket of chain A and chain B are −10.5 kcal/mol and −11.5 kcal/mol, respectively. Conversely, the best binding energies calculated for **1a** and **1b** in the S2 pocket of chain A are −11.0 kcal/mol and −12.2 kcal/mol, respectively, still below the value of **6** but above the values found for **1a** and **1b** inside S1.

5. The Noncanonical Binding Site (S2). The S2 site is flanked by the loop H1−H2 and helix 3, the helix 5, and helix 8. The flexible loop H1−H2 constitutes the

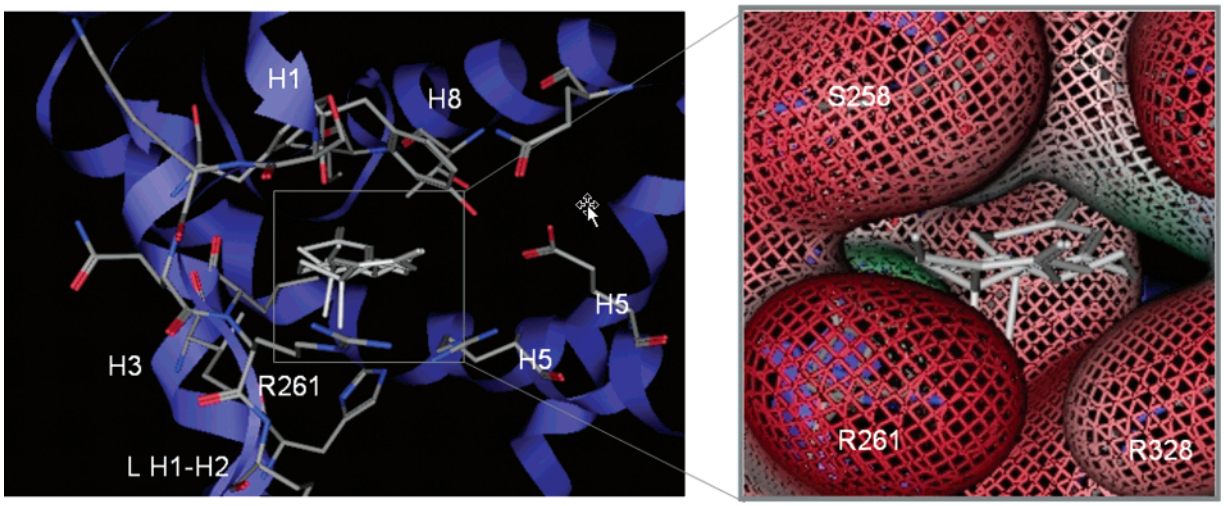

Figure 4. Lowest energy binding position (cluster 1) of **1a** inside the noncanonical binding site (S2) in its molecular surrounding. Left: General view of microdomains involved. Right: Molecular surface (Gauss accessible) of the S2 site.

Table 4. Interacting Residues in the Noncanonical Binding Site S2, Residue Number, Structural Element, and Interacting Atoms[a]

residue	structural element	interacting atoms
Tyr Y257	H1	C1′-C6′, 4′-OH
Ser S258	L (H1−H2)	CO, Cα, Cβ, NH
Lys K259	L (H1−H2)	NH
Glu Q260	L (H1−H2)	CO
Arg R261	L (H1−H2)	NH, Cα-N(ter), CO
Met M262	L (H1−H2)	NH
His H291	H3	C3′, N4′
Ile I294	H3	Cδ
Leu L295	H3	complete
Phe F298	H3	Cβ, C1′-C3′, C6′
Arg R328	H5	Cβ-N(ter)
Glu E331	H5	O(ter)
Gln Q376	H8	O(ter)
Thr T383	H8	Cβ, Cγ
Ile I387	H8	Cδ
volume	650.0 Å^3	

[a] 4.5 Å Distance from docking position of the first cluster for **1a** in Chain A, H = Helix, L (H1−H2) = loop between Helix 1 and Helix 2).

outer part of S2 (Figure 4). This pocket has a volume of 650 Å^3 in chain A and 520 Å^3 in chain B and is apparently formed by seven residues, namely Y257 (final residue of helix 1), S258 and R261, of the loop H1−H2, L295 and F298 of helix 3, R328 of helix 5, and T383 of helix 8.

Residues involved in ligand binding in the first and the second cluster of **1a** and the first cluster of **1b**, constituting S2, are listed in Table 4.

As mentioned above, the first two docking positions for **1a** are found in the S2 site. In its lowest energy position, **1a** is pointing with the 3-carbonyl-group toward helix 5 and helix 8 inside the receptor structure, where no polar interaction partner is found in an environment of 4.0 Å (Figure 5). The nearest nonpolar side chains are the δ-carbon of L295 (2.88 Å, helix 5) and the β-carbon of T383 (2.95 Å, helix 8).

The 16-carbonyl function of **1a** is solvent accessible, flanked by two arginines (R261 of loop H1−H2 and R328 of H5) in a distance of 4.91 Å and 5.10 Å, respectively. The β-face of the ligand is directed toward M262 and H291, and the α-face is shielded by the almost coplanar helix 1 Y257, the hydroxy function of which is bound to

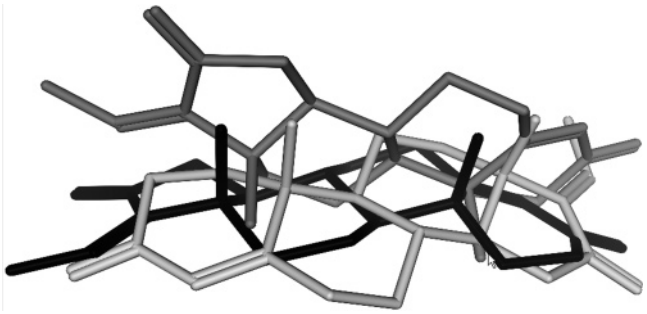

Figure 5. Occupancy of the S2 site: First (black) and second cluster (dark-grey) of **1a** in FXR (E_{bind}: −10.9 kcal/mol, abundancy = 12%, 10.5 kcal/mol, abundancy = 5%) and first cluster (bright gray) of **1b** in FXR (E_{bind}: −12.1 kcal/mol, abundancy = 7%).

the carboxylate of E331 backbone carbonyl of Y257 of helix 1, thus forming a hydrogen bond (distance: 3.31 Å, $N_{ter}-O_{ter}$).

In the second docking cluster, **1a** approaches the ϵ-NH of R261 with its 16-carbonyl and 21-methyl-group (Figure 5, distance (C−H) 3.8 Å and 2.2 Å, respectively). The β-face is directed toward helix 3, due to the fact that the ligand is turned by 120° clockwise along the axis described by O3 and O16. It shows a van der Waals interaction of its 19-methyl group with the γ-methyl moiety of isoleucine I294 (distance (C−C) = 3.8 Å).

Also the first docking cluster of **1b** is located in the noncanonical binding site S2, where it is found in a position similar to that of **1a**. With respect to the corresponding position of **1a**, **1b** is turned around about 180° (Figure 5).

6. Differences between Chain A and B in the Accessibility of the Noncanonical Binding Site S2. The differences in the accessible volume of the noncanonical binding site S2 between chain A and B is caused by a conformational change in the loop H1−H2. Visual inspection of the superimposed structures of chain A and B in this particular region displayed differences in the orientation of some of the side chains in the loop H1−H2 (Figure 6 left). This is in particular the case for R261, whose ψ- and φ-angles differ substantially between the chain A and chain B (Table 5). When comparing the φ- and ψ-angles in loop H1−H2 in chains A and B, the

Table 5. Loop Region between Helix 1 and 2 in Chains A and B, Comparison of the φ and ψ Angles of the Residues, and Direction of the Side Chains

	Φ	ψ	direction
	Chain A		
Tyr Y257	−40°	−60°	inside
Ser S258	+40°	−100°	outside
Lys K259	−70°	−80°	outside
Gln Q260	−70°	−50°	outside
ArgR 261	+140°	+60°	outside
Met M262	+130°	−60°	inside
Pro P263	+140°	−60°	−
	Chain B		
Tyr Y257	−40°	−70°	inside
Ser S258	−15°	−80°	outside
Lys K259	−40°	−50°	outside
Gln Q260	+110°	−140°	outside
Arg R261	+90°	−110°	inside
Met M262	+40°	+30°	inside
Pro P263	±180°	−50°	−

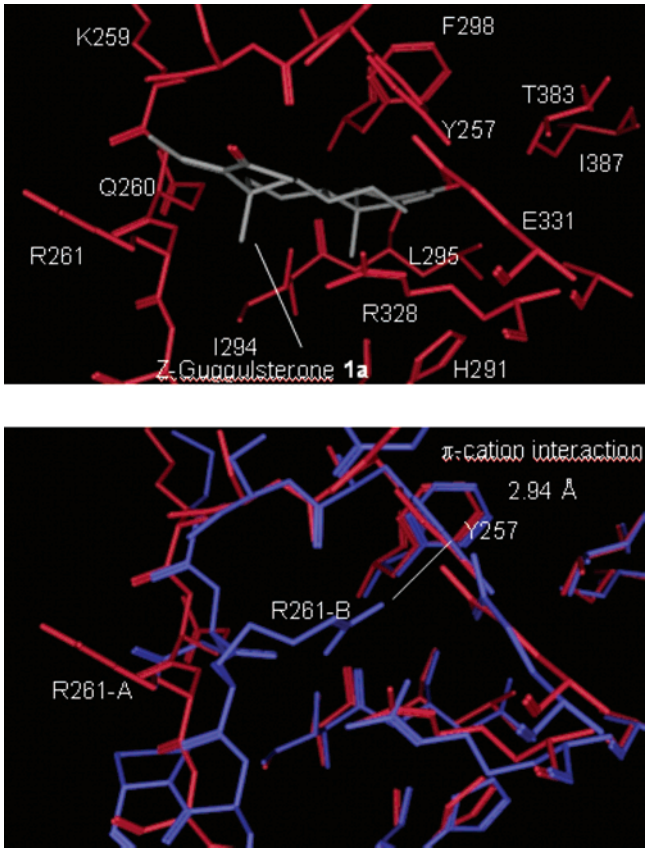

Figure 6. The noncanonical binding site (S2) in chain A (red) and chain B (blue). Above: In chain A, **1a** and **1b** can entry because of the disposition of R261, shown as example cluster 1 of **1a**. Below: Superimposition of chain A (red) and chain B (blue). In chain B the side chain (dark gray) of R261 is entering the cavity of the noncanonical binding site (S2). The guanidinium group of R261 (black) shows a π−cation interaction with the aromatic system of Y257 (distance: 2.94 Å).

increment of R261 is +150°, while it is in the range between 0° and +100° for the flanking microarray Y257−P263.

In chain A, R261 is fully exposed to the solvent, while in chain B, the side chain of this residue is projecting into the inside the noncanonical binding site S2, where it interacts with the backbone carbonyl of Y257 of helix 1, thus forming a π−cation interaction (Figure 6 right).

As a consequence, the accessibility for **1** of the noncanonical binding site S2 is diminished in chain B. In the protein complex, in which the second noncanonical coactivator peptide is bound to helix 3, Q264 interacts with Asn 2′ of the coactivator peptide (distance: 4.08 Å, N_{ter}−N_{ter}). Here, R261 is directed inside the noncanonical binding site S2 (φ: +90°, ψ: −110°) and binds the terminal nitrogen of its guanidinium group to the aromatic system of Y257 in terms of an edge to face π−cation interaction (distance: N_{ter}−C_{arom} 2.91 Å).

7. Binding Positions Located Inside the Canonical Binding Site S1. The docking positions of **1a** and **1b** located inside the canonical binding site S1 of chain A (cluster 3−5 of **1a** and cluster 2−5 of **1b**; Table 2) are found inside the volume described by the van der Waals radius of **6** cocrystallized in FXR (Figure 3, right side). The distribution of docking positions found in chain B is matching to the distribution of docking positions found inside the canonical binding site S1 in chain A. In all clusters inside S1, **1** approaches the residues M325 of helix 5. Neither **1a** nor **1b** significantly approached helix 12 residues in general and W464 in particular. Also polar interactions of the 3-carbonyl group of the **1** with elements of the trigger Y358, H444, or W464 were not found. On the contrary, in some of the clusters, ring A of **1** is found inside the volume occupied by the 6-ethyl group of **6** described in the crystal structure of FXR, i.e., the pocket described by Y358, F363, and I354. In this docking position the 16-carbonyl function of **1** interacts with the sulfur of M287 in helix 3. In chain A only in the fifth cluster of **1a** and the third cluster of **1b** is a hydrogen bond between the 3-carbonyl moiety and the phenolic hydroxy-group of Y358 observed (distance: 2.52 Å, O−O). Here the distance between ring A of the **1** in their docking positions and the aromatic system of W464 is found to be 4.00 Å (C−C). In this position a simultaneous interaction of the 16-carbonyl-group of **1** with M262 (loop H1−H2) is impossible, as the distance between the 16-carbonyl and the sulfur of M262 is larger than 8 Å. On the other hand, in clusters in which **1** interacts with residues of loop H1−H2 (i.e. mainly the side chain of M262) the ligands are reciprocally not able to interact with H11 or H12 residues. In conclusion the positions belonging to the clusters inside S1 of either **1a** and **1b** display some of the interactions found with **6**, but do not encompass the full extent of interaction displayed by **6** in the crystal of 1OSV.

Discussion

FXR is activated by bile acids, as exemplified by **2** or **6**. Bile acids are amphiphilic molecules characterized by a concave hydrophilic β-face and a convex lipophilic α-face. This amphiphilic character is not only responsible for the bile acid's ability to form micelles, but it also accounts for the proper recognition and activation of the FXR receptor. Lacking both the amphiphilic character and the distinct bile acid's stereochemistry (cis junction of ring A and B), **1** is unable to reproduce the full pattern of binding interactions displayed by **2** or **6** when binding to FXR.[41,42] Thus, the lack of FXR-activating properties of **1** deserves no additional comments. The antagonism of **1** toward FXR in FRET-based coactivator recruitment assays is more intriguing, es-

pecially when evaluated in conjunction with its ability to selectively enhance the FXR-agonist-induced expression of the bile salt export pump (BSEP), one of the target genes for FXR. Classically, NR antagonists are more voluminous than their cognate agonists, and the antagonism is described by the antagonist's ability to destabilize the receptor's active conformation, where the crucial helix H12 is packed toward the core of the protein and allows coactivator binding. **1** cannot fit this scheme, as it is considerably smaller than **2**. Indeed, our docking studies indicate that both **1a** and **1b** can be positioned into the bile acid binding pocket (S1, Table 2, cluster 3−5 of **1a** and cluster 2−5 of **1b**; Table 3, all clusters of either **1a** or **1b**), but scarce interactions with the trigger's microstructure which stabilizes H12 are apparent. Thus, alternative concepts for antagonism of **1** have to be proposed. In this regard, we found it very interesting to observe that in chain A, but not in chain B, both **1a** and **1b** can be positioned into an unprecedented binding pocket, that we have called S2. Furthermore, for both **1a** and **1b**, this alternative binding position in chain A is endowed with the lowest binding energy.

According to our docking results, at least three different hypotheses on antagonism of **1** can be explained. First of all, both in chain A and chain B, **1a** and **1b** can be positioned inside the canonical S1 binding pocket. Thus, **1** can simply compete with **2** or other agonists. The predicted binding energies for **1a** and **1b** are more than 4 kcal/mol weaker than for **6** and are somehow compatible with the relatively low antagonist potency at FXR. Considering the binding of **1a** and **1b** in the canonical binding site S1, neither **1a** and **1b** are able to interact simultaneously with Y358 of helix 11 and M262 of the loop H1−H2, due to their shorter length in comparison with **6**. Therefore, **1a** and **1b** are unable to stabilize both the active conformation of helix 12 and the loop H1−H2 at the same time.

The identification of the alternative binding disposition on the S2 site, however, put forward alternative hypotheses that, if proved, can constitute a new concept for NR antagonism. Thus, the S2 site identified in chain A may constitute the first meta-binding site for ligands entering the canonical binding pocket. Indeed, the region near H3 was recently recognized as the putative entrance to the S1 site in the peroxisome proliferator activated receptor α (PPARα).[43,44]

Following this concept, we assumed the channel formed by the residues M262, M287, H291, R328, and F333 is responsible for the entrance of the ligand to S1, when H12 is kept in its activating position stabilized by the trigger Y358 H444 W464. The location of a noncanonical binding site S2 for **1** in direct proximity to the entry point of agonists in FXR allows us to think of additional possible mechanisms of antagonism of **1a** and **1b**. In binding to the backside of the residues R328 and I294, which form the upper part of this entrance channel, **1** may move these side chains into the channel and might additionally block the entrance of the receptor.

According to this idea, we proposed a third possibility for **1** antagonism at FXR. The flexible loop H1−H2 displays some impact on the occupancy of the noncanonical binding site S2. In this microdomain the orientation of R261 is different in chains A and B (chain A: φ: +140°, ψ: +60° vs chain B: φ: +90°, ψ: −110°). In chain A, the noncanonical binding site S2 is accessible for either **1a** and **1b** and the side chain of R261 is directed to the receptor outside. Its ω-guanidinium group does not show an apparent interaction partner at a distance of 6.0 Å, but is possibly able to interact with the i+3-residue Q264 (distance 6.19 Å) due to its conformational flexibility. Differently in chain B, R261 is directed into the receptor structure, i.e., into the noncanonical binding site S2, where it interacts with Y257. Conclusively, in chain B the canonical binding site S2 is not accessible for either **1a** and **1b** for steric reasons.

In reverse, the occupancy of S2 by **1** possibly accounts for a conformational change in loop H1−H2. Binding of **1** to S2 may disrupt the π−cation interaction between R261 and Y257 and then induce a disposition of R261 from the inside of S2 to the outside of the receptor similar to the conformation observed in chain A. In this conformation the ω-guanidinium moiety of R261 is enabled to interact with the carboxylate of the i+3-residue Q264. This interaction then possibly leads to a conformational change of the side chain of Q264 and prevents its carboxylate moiety from an interaction with Asn2′ of coactivator protein II.[45] This may result in altering the binding properties of the latter. In conclusion, binding of **1** to S2 possibly can modify the coactivator II assembly of FXR, moving the equilibrium from the state of FXR described by chain B (FXR with two coactivators) to that of chain A (FXR with one coactivator).

Taken together, the binding of either **1a** and **1b** to a noncanonical binding site S2 might be a clue for understanding the antagonistic properties in FXR through stabilizing the chain A-like conformation of FXR. Recent molecular dynamic studies described the crucial role of Q264 as one of the residues involved in the binding of coactivator II, so that this residue may account as an interacting partner for R261, when the coactivator II is released.[45] Furthermore, starting from the chain B crystal structure of 1OSV containing no coactivators, the final conformation of the explicit loop H1−H2 resembled its conformation in chain A, in which the side chain of R261 is directed to the receptor outside. **1** binding to the S2 site may in that respect lead to coactivator II disassembly and stabilization of chain A-like FXR conformations. Additional to its possible binding in the S1 site, the existence of a S2 site may provide further insight in the mode of modulating FXR by guggulsterone-like compounds.

Acknowledgment. Intercept Pharmaceuticals (NY) is acknowledged for financial support.

References

(1) Singh, R. B.; Niaz, M. A.; Ghosh, S. Hypolipidemic and antioxidant effects of Commiphora mukul as an adjunct to dietary therapy in patients with hypercholesterolemia. *Cardiovasc. Drugs Ther.* **1994**, *4*, 659−664.
(2) Sinal, C. J.; Gonzalez, F. J. Guggulsterone: an old approach to a new problem. *Trends Endocrinol. Metab*. **2002**, *13*, 275−276.
(3) Wang, X.; Greilberger, J.; Ledinski, G.; Kager, G.; Paigen, B.; Jürgens, G. The hypolipidemic natural product Commiphora mukul and its component guggulsterone inhibit oxidative modification of LDL. *Atheriosclerosis* **2004**, *172*, 239−246.
(4) Satyavati, G. V. Gum guggul (Commiphora mukul)-the success story of an ancient insight leading to a modern discovery. *Indian. J. Med. Res*. **1988**, *87*, 327−335.

(5) Szapary, P. O.; Wolfe, M. L.; Bloedon, L. T.; Cucchiara, A. J.; DerMarderosian, A. H.; Cirigliano, M. D.; Rader, D. J. Guggulipid for the treatment of hypercholesterolemia: a randomized controlled trial. *JAMA* **2003**, *290*, 765−772.
(6) Urizar, N. L.; Moore, D. D. Guggulipid: a natural cholesterol-lowering agent. *Annu. Rev. Nutr.* **2003**, *23*, 303−313.
(7) Burris, T. P.; Montrose, C.; Houck, K. A.; Osborne, H. E.; Bocchinfuso, W. P.; Yaden, B. C.; Cheng, C. C. et al. The Hypolipidemic Natural Product Guggulsterone is a Promiscuous Steroid Receptor Ligand. *Mol Pharmacol*. **2005**, *67*, 948−954.
(8) Urizar, N. L.; Liverman, A. B.; Dodds, D. T.; Silva, F. V.; Ordentlich, P.; Yan, Y. et al. A natural product that lowers cholesterol as an antagonist ligand for FXR. *Science* **2002**, *296*, 1703−1706.
(9) Cui, J.; Huang, L.; Zhao, A.; Lew, J. L.; Sahoo; S.; Meinke; P. T. et al. Guggulsterone is a farnesoid X receptor antagonist in coactivator association assays but acts to enhance transcription of bile salt export pump. *J. Biol. Chem*. **2003**, *278*, 10214−10220.
(10) Wu, J.; Xia, C.; Meier, J.; Li, S.; Hu, X.; Lala, D. S. The hypolipidemic natural product guggulsterone acts as an antagonist of the bile acid receptor. *Mol. Endocrinol*. **2002**, *16*, 1590−1597.
(11) Owsley, E.; Chiang, Y. L. Gugulsterone antagonizes farnesoid X receptor induction of bile salt export pump but activates pregnane X receptor to inhibit cholesterol 7alpha-hydroxlase gene. *Biochem. Biophys. Res. Commun*. **2003**, *304*, 191−195.
(12) Parks, D. J.; Blanchard, S. G.; Bledsoe, R. K.; Chandra, G.; Consler, T. G.; Kliewer, S. A.; Stimmel, J. B.; Willson, T. M.; Zavacki, A. M.; Moore, D. D.; Lehmann, J. M. Bile acids: natural ligands for an orphan nuclear receptor. *Science* **1999**, *284*, 1365−1368.
(13) Makishima, M.; Okamoto, A. Y.; Repa, J. J.; Tu, H.; Learned, R. M.; Luk, A. et al. Identification of a nuclear receptor for bile acids. *Science* **1999**, *284*, 1362−1365.
(14) Wang, H.; Chen, J.; Hollister, K.; Sowers, L. C.; Forman, B. M. Endegenous bile acids are ligands for the nuclear receptor FXR/BAR. *Mol. Cell* **1999**, *3*, 543−553.
(15) Maloney, P. R.; Parks, D. J.; Hafner, C. D.; Fivush, A. M.; Chandra, G.; Plunket, K. D.; Creech, K. L. et al. Identification of a chemical tool for the orphan nuclear receptor FXR. *J. Med. Chem*. **2000**, *43*, 2971−2974.
(16) Russell, D. W. The enzymes, regulation, and genetics of bile acid synthesis. *Annu. Rev. Biochem*. **2003**, *72*, 137−174.
(17) Pellicciari, R.; Costantino, G.; Camaioni, E.; Sadeghpour, B. M.; Entrena, A.; Willson, T. M.; Fiorucci, S.; Clerici, C.; Gioiello, A. 6alpha-ethyl-chenodeoxycholic acid (6-ECDCA), a potent and selective FXR agonist endowed with anticholestatic activity. *J. Med. Chem*. **2002**, *45*, 3569−3572.
(18) Willson, T. M.; Jones, S. A.; Moore, J. T.; Kliewer, S. A. Chemical genomics: functional analysis of orphan nuclear receptors in the regulation of bile acid metabolism. *Med. Res. Rev*. **2001**, *21*, 513−522.
(19) Downes, M.; Verdecia, M. A.; Roecker, A. J.; Hughes, R.; Hogenesch, J. B.; Kast-Woelbern, H. R. A chemical, genetic, and structural analysis of the nuclear bile acid receptor FXR. *Mol. Cell*. **2003**, *11*, 1079−1092.
(20) Bramlett, K. S.; Yao, S.; Burris, T. P. Correlation of farnesoid X receptor coactivator recruitment and cholesterol 7alpha-hydroxylase gene repression by bile acids. *Mol. Genet. Metab*. **2000**; *71*, 609−615.
(21) Chiang, J. Y.; Kimmel, R.; Weinberger, C.; Stroup, D. Farnesoid X receptor responds to bile acids and represses cholesterol 7 alpha-hydroxylase gene (CYP7A1) transcription. *J. Biol. Chem*. **2000**, *275*, 10918−10924.
(22) Goodwin, B.; Jones, S. A.; Price, R. R.; Watson, M. A.; McKee, D. D.; Moore, L. B. et al. A regulatory cascade of the nuclear receptor FXR, SHP-1 and LRH-1 represses bile acid biosynthesis. *Mol. Cell* **2000**, *6*, 517−526.
(23) Lu, T. T.; Makishima, M.; Repa, J. J.; Schoonjans, K.; Kerr, T. A.; Auwerx, J.; Mangelsdorf, D. J. Molecular basis for feedback regulation of bile acid synthesis by nuclear receptors. *Mol. Cell* **2000**, *6*, 507−515.
(24) Zhang, M.; Chang, J. Y. Transcriptional regulation of the human sterol 12 alpha-hydroxylase gene (CYP8B1): Roles of hepatocyte nuclear factor 4alpha in mediating bile acid repression. *J. Biol. Chem*. **2001**, *276*, 41690−41699.
(25) Denson, L. A.; Sturm, E.; Echevarria, W.; Zimmerman, T. L.; Makishima, M.; Mangelsdorf, D. J.; Karpen, S. J. The orphan nuclear receptor, SHP, mediates bile acid-induced of the rat bile acid transporter, NTCP. *Gastroenterology* **2001**, *121*, 140−147.
(26) Ananthanarayanan, M.; Balasubramanian, N.; Makishima, M.; Mangelsdorf, D. J.; Suchy, F. J. Human bile acid salt export pump promoter is transactivated by the farnesoid X receptoer/bile acid receptor. *J. Biol. Chem*. **2001**, *276*, 28857−28865.
(27) Huang, L.; Zhao, A. Lew, J. L.; Zhang, T.; Hrywna, Y. Thompson, J. R. et al. Farnesoid X receptor activates transcription of the phospholipids pump MDR3. *J. Biol. Chem*. **2003**, *278*, 51085−51090.
(28) Kast, H. R.; Goodwin, B.; Tarr, P. T.; Jones, S. A.; Anisfeld, A. M.; Stoltz, C. M. et al. Regulation of multidrug resistance-associated protein 2 (ABCC2) by the nuclear receptors pregnane X receptor, farnesoid X-activated receptor, and constitutive androstane receptor. *J. Biol. Chem*. **2002**, *277*, 2908−2915.
(29) Grober, J.; Zaghini, I.; Fujii, H.; Jones, S. A.; Kliewer, S. A.; Willson, T. M. et al. Identification of a bile acid-responsive element in the human ileal bile acid-binding protein gene. Involvement of the farnesoid X receptor/9-cis-retinoic acid receptor heterodimer. *J. Biol. Chem*. **1999**, *274*, 29749−29754.
(30) Urizar, N. L.; Dowhan, D. H.; Moore, D. D. The farnesoid X-activated receptor mediates bile acid activation of phospholipids transfer protein gene expression. *J. Biol. Chem*. **2000**, *275*, 39313−39317.
(31) Claudel, T.; Sturm, E.; Duez, H.; Torra, I. P.; Sirvent, A.; Kosykh, V. et al. Bile acid-activated nuclear receptor FXR suppresses apolipoprotein A−I transcription via a negative FXR response element. *J. Clin. Invest*. **2002**, *109*, 961−971.
(32) Kast H. R.; Nguyen, C. M.; Sinal, C. J.; Jones, S. A.; Laffitte, B. A. et al. Farnesoid X-activated receptor induces apolipoprotein C−II transcription: A molecular mechanism linking plasma triglyceride levels to bile acids. *Mol. Endocrinol*. **2001**, *15*, 1720−1728.
(33) Claudel, T.; Inoue, Y.; Barbier, O.; Duran-Sandoval, D.; Kosykh, V.; Fruchart, J. et al. Farnesoid X receptor agonists suppress hepatic apolipoprotein CIII expression. *Gastroenterology* **2003**, *125*, 544−555.
(34) Zhao, A.; Lew, J. L.; Huang, Y.; Yu, J.; Zhang, T.; Hrywna, Y. et al. Human kininogen gene is transactivated by the farnesoid X receptor. *J. Biol. Chem*. **2003**, *278*, 28765−28770.
(35) Fiorucci, S.; Antonelli, E.; Rizzo, G.; Renga, B.; Mencarelli, A.; Riccardi, L.; Orlandi, S.; Pellicciari, R.; Morelli, A. The nuclear receptor SHP mediates inhibition of hepatic stellate cells by FXR and protects against liver fibrosis. *Gastroenterology* **2004**, *127*, 1497−1512.
(36) Zhao, A.; Yu, J.; Lew, J. L.; Huang, L.; Wright, S. D.; Cui, J. Polyunsaturated fatty acids are FXR ligands and differentially regulate expression of FXR targets. *DNA Cell Biol*. **2004**, *23*, 519−526.
(37) Xu, E.; Stanley, T. B.; Montana, V. G.; Millard, H. L.; Shearer, B. G.; Cobb, J. E.; McKee D. D. Structural basis for antagonist-mediated recruitment of nuclear co-repressors by PPARalpha. *Nature* **2002**, *415*, 813−817.
(38) Brzozowski, A. M.; Pike, A. C. W.; Dauter, Z.; Hubbard, R. E.; Bonn, T.; Engström, O.; Öhman, L. Molecular basis of agonism and antagonism in the oestrogen receptor. *Nature* **1997**, *389*, 753−753.
(39) Shiau, A. K.; Barstad, D.; Loria, P. M.; Cheng, L.; Kushner, P. J.; Agard, D. A.; Greene, G. L. The structural basis of estrogen receptor/coactivator recognition and the antagonism of this interaction by tamoxifen. *Cell* **1998**, *95*, 927−937.
(40) Mi, L. Z.; Devarakonda, S.; Harp, J. M.; Han, O.; Pellicciari, R.; Willson, T. M. et al. Structural basis for bile acid binding and activation of the nuclear receptor FXR. *Mol. Cell*. **2003**, *11*, 1093−1100.
(41) Costantino, G.; Macchiarulo, A.; Entrena-Guadix, A.; Camaioni, E.; Pellicciari, R. Binding mode of 6ECDCA, a potent bile acid agonist of the farnesoid X receptor (FXR). *Bioorg. Med. Chem. Lett*. **2003**, *13*, 1865−1868.
(42) Pellicciari, R.; Costantino, G.; Camaioni, E.; Sadeghpour, B. M.; Entrena, A.; Willson, T. M.; Fiorucci, S.; Clerici, C.; Gioiello, A. Bile acid derivatives as ligands of the farnesoid X receptor. Synthesis, evaluation, and structure−activity relationship of a series of body and side chain modified analogues of chenodeoxycholic acid. *J. Med. Chem*. **2004**, *47*, 4559−4569.
(43) Sheu, S. H.; Taner, K.; Waxman, D. J.; Vadja, S. Exploring the binding site structure of the PPARγ ligand-binding domain by computional solvent mapping. *Biochemistry* **2005**, *44*, 1193−1209.
(44) Cronet, P.; Petersen, J. W. F.; Folmer, R.; Blomberg, N.; Sjöblorn, K.; Karlsson, U. et al. Structure of the PPARα and -γ Ligand Binding Domain in Complex with AZ 242; Ligand Selectivity and Agonist Activation in the PPAR Family. *Structure* **2001**, *9*, 699−706.
(45) Costantino, G.; Entrena-Guadix, A.; Macchiarulo, A.; Gioiello, A.; Pellicciari, R. Molecular dynamics simulation of the ligand binding domain of farnesoid X receptor. Insights into helix-12 stability and coactivator peptide stabilization in response to agonist binding. *J. Med. Chem.* **2005**, *48*, 3251−3259.

JM0505056